

Nuclear structure of even lead isotopes by the (p, t) reaction

M. Takahashi,* T. Murakami, and S. Morita†

Department of Physics, Faculty of Science, Tohoku University, Sendai 980, Japan

H. Orihara

Cyclotron and Radioisotope Center, Tohoku University, Sendai 980, Japan

Y. Ishizaki

Institute for Nuclear Study, University of Tokyo, Tanashi 188, Japan

H. Yamaguchi

Faculty of General Education, Tokushima University, Tokushima 770, Japan

(Received 22 November 1982)

The $^{208,206,204}\text{Pb}(p, t)^{206,204,202}\text{Pb}$ reactions have been studied at an incident energy of 51.9 MeV. With the aid of distorted-wave Born approximation calculations a number of spin and parity assignments were made. Systematic trends were observed in the experimental excitation energy of individual levels in the residual nuclei and transition strengths for three reactions. These results are compared with predictions from the shell-model wave functions. The overall agreement is satisfactory.

NUCLEAR REACTIONS $^{208,206,204}\text{Pb}(p, t)$, $E_p = 51.9$ MeV; measured $\sigma(E_t, \theta)$; deduced energies, spins, parities, and strengths; DWBA analysis; enriched targets and shell-model calculation.

I. INTRODUCTION

It has been expected that the nuclei in a region of doubly closed shells should be fairly well described in terms of the shell model. Regarding ^{206}Pb nuclei, True and Ford^{1,2} calculated the shell-model wave functions using a phenomenological nucleon-nucleon residual interaction, and Herling and Kuo³ calculated them on the basis of the realistic Hamada-Johnston nucleon-nucleon interaction. The shell-model calculation for the other lead isotopes has been done by Lanford and McGrory⁴ only in a limited region of the excitation energy of ^{204}Pb .

Smith *et al.*⁵ studied the $^{208}\text{Pb}(p, t)^{206}\text{Pb}$ reaction, and compared the experimental excitation energies and the transition strengths for natural-parity levels below 3.4 MeV with the predictions from a set of shell-model wave functions. They have concluded that the wave functions derived from shell-model calculations provide a quite satisfactory description of the experimental results and that the singlet-even central interaction is the dominant part of the residual interaction.

Lanford investigated⁶ the (p, t) reactions on ^{208}Pb , ^{206}Pb , and ^{204}Pb at $E_p = 35$ MeV and reported the

spins, parities, excitation energies, and transition strengths for levels below 4.2 MeV in ^{206}Pb , and below 3.2 MeV in ^{204}Pb and ^{202}Pb . They applied the two-neutron-transfer sum rule of Bayman and Clement⁷ to those data, and have shown that the observed drastic increase in the (p, t_0) cross section with the decrease in the mass number from ^{208}Pb to ^{204}Pb can be explained from general features of the shell model for these nuclei.

Orihara *et al.*⁸ studied the (p, t) reaction on lead isotopes and reported that the most prominent peaks in the triton spectra of $^{208,207,206,204}\text{Pb}(p, t)^{206,205,204,202}\text{Pb}$ reactions were identified as $L = 6$ transfers and that the relatively strongly populated states at about $E_x = 5$ MeV in ^{206}Pb and ^{204}Pb were $J^\pi = 11^-$ states, i.e., $L = 11$ transfer.

We investigate here the $^{208,206,204}\text{Pb}(p, t)$ reactions with a high-energy incident beam and study the high-spin states of up to 11^- in higher excited states. We have also obtained the wave functions of natural parity states for $^{206,204,202}\text{Pb}$ in the framework of the shell model, and comparisons between these experimental and theoretical results are presented for excitation energies and transition strengths for individual transitions.

II. EXPERIMENTAL PROCEDURE

Beams of 51.9-MeV protons for this experiment were provided from the synchrocyclotron of the Institute for Nuclear Study of Tokyo University. Emitted tritons were momentum analyzed with the magnetic analysis system and were detected with an array of 200 proportional counters followed by a large plastic-scintillation-counter system.⁹ The 200 proportional counters serve as position detectors, and they form counter telescopes in combination with the scintillation counters. The overall energy resolution for the tritons of interest is about 90 keV.

The targets of ^{208}Pb and ^{206}Pb were metallic foils of 4- and 5-mg/cm² thickness, respectively. The ^{204}Pb target was 2 mg/cm² thick and prepared by centrifugal settling of PbO onto a Mylar backing. These targets were enriched to more than 99%. The thicknesses were determined by weighing and also by comparison of the yields of elastically scattered protons with the predictions obtained from the optical model by using parameters given by Becchetti and Greenlees.¹⁰ The consistency between the values

obtained from these methods was about 10%. The error of the absolute cross section of the ground state transition is estimated to be less than 20%, where the main part comes from the uncertainty of the solid angle of each counter on the focal plane of the magnetic spectrograph.

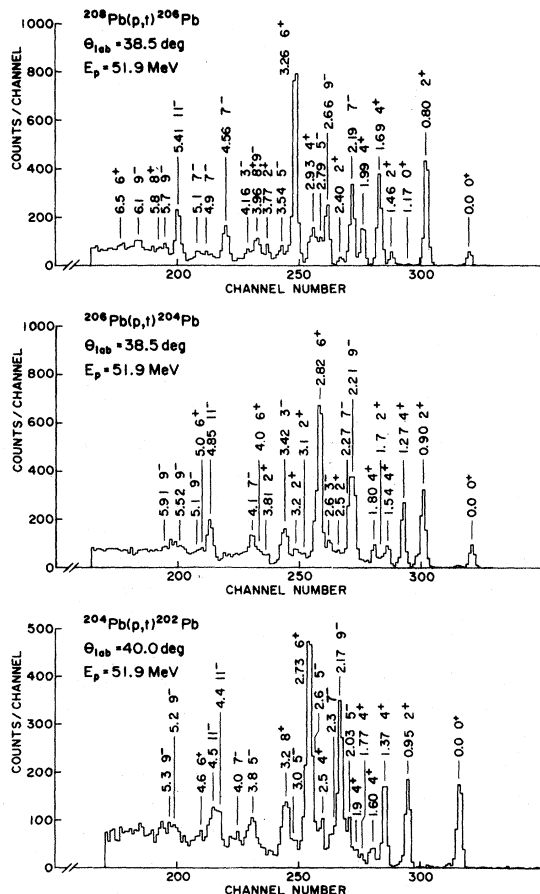


FIG. 1. Typical triton-momentum spectra.

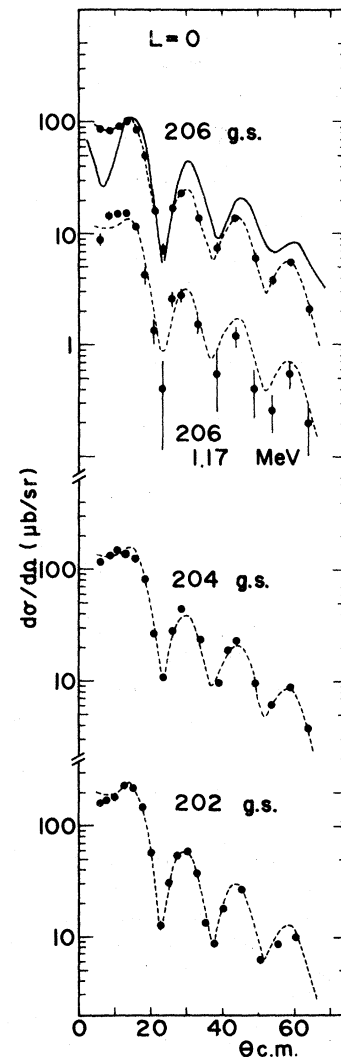


FIG. 2. Experimental and theoretical angular distributions for the $L=0$ transition obtained from the (p,t) reaction on even lead isotopes. The solid line is the DWBA predictions calculated from the code DWUCK-4 as explained in the text. The broken line is to guide the eye to see the experimental angular distribution of tritons leading to the lowest $J^\pi=0^+$ state (g.s.) in ^{206}Pb .

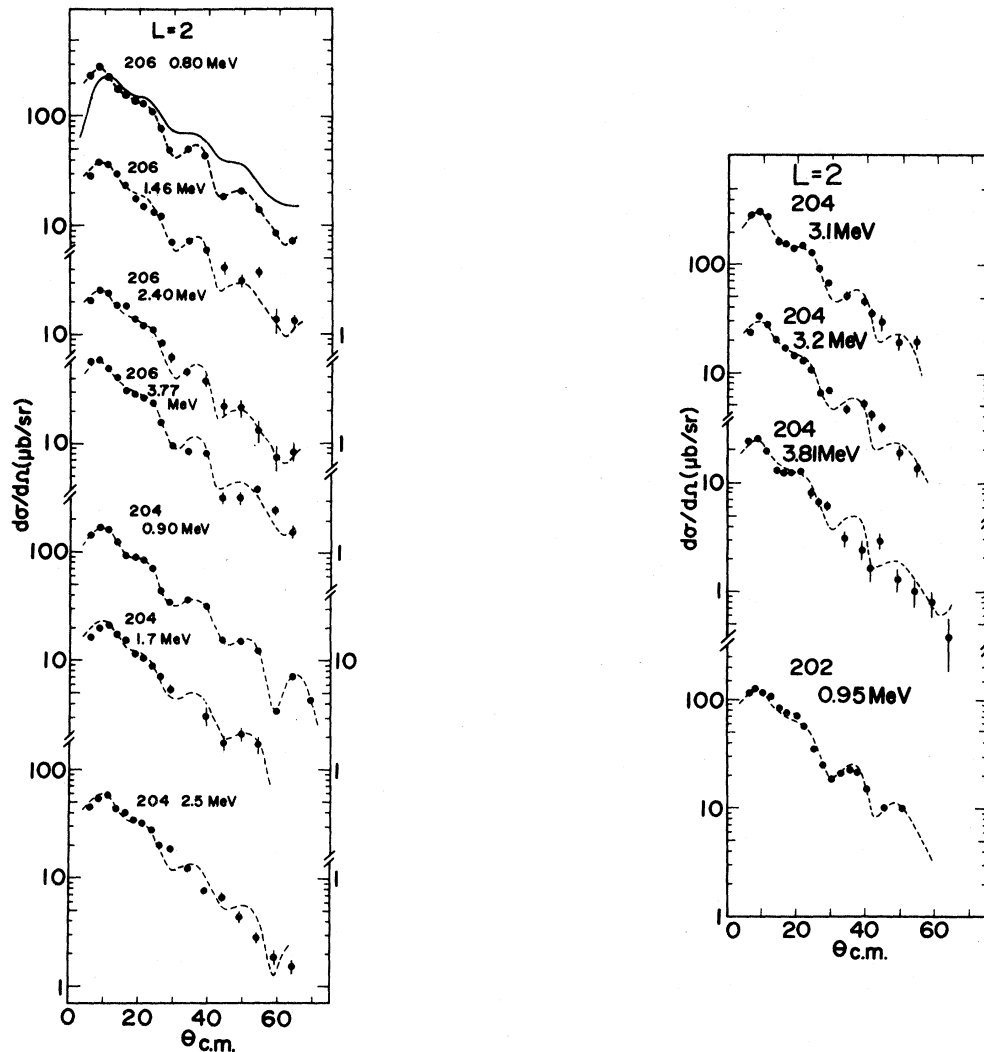


FIG. 3. Differential cross sections for $L=2$ transitions. The broken line is to guide the eye to show the angular distribution of tritons leading to the lowest 2^+ state (0.804 MeV) in ^{206}Pb .

III. RESULTS

The triton-momentum spectra for the ^{208}Pb , ^{206}Pb , and ^{204}Pb targets are shown in Fig. 1, where excitation energies and spin-parity assignments are also indicated. The observed angular distributions are presented in Figs. 2–11 for each transfer angular momentum L . A transfer- L assignment was done by the aid of DWBA calculations and by comparisons of the individual angular distribution for the transition of interest with that for the transition to the known state (say an experimental angular distribution). Here, it should be worth mentioning that the angular distribution of differential cross sections shows a similar shape regardless of the choice of the two-hole configuration in almost all cases. In Figs. 5–9, comparisons of experimental angular distribu-

tion shapes for alternate values of the transferred L are shown for the tritons leading to the lowest state within the given J^π . Owing to the relatively poor experimental resolution, such definite assignments given here may be claimed to be ambiguous. It should be emphasized that angular distributions for each triton group are well fitted by the theoretical and/or experimental angular distribution with a few exceptions, i.e., the 1.77 MeV state assigned to be 4^+ in ^{202}Pb , and 4.0 and 5.7 MeV states in ^{206}Pb labeled as $L=9$ transitions. For the first one, the possibility of a 2^+ state is not rejected completely. The second one is discussed later on, and the third one may contain low- L components in the differential cross sections at forward angles.

A computer program has been employed to find peak energies and to integrate peak areas. The error

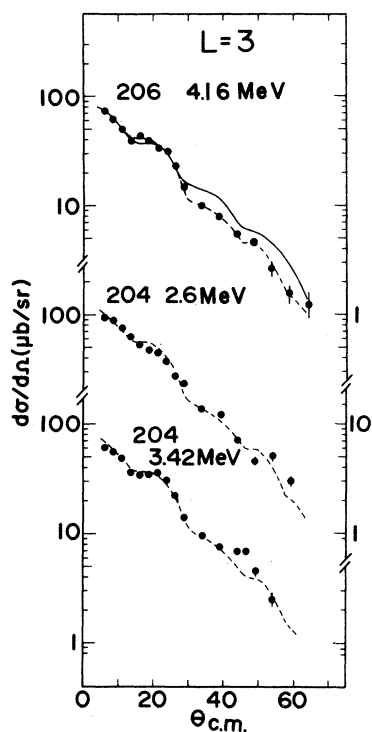


FIG. 4. Experimental differential cross sections for the $L=3$ transitions. See the captions to Figs. 2 and 3.

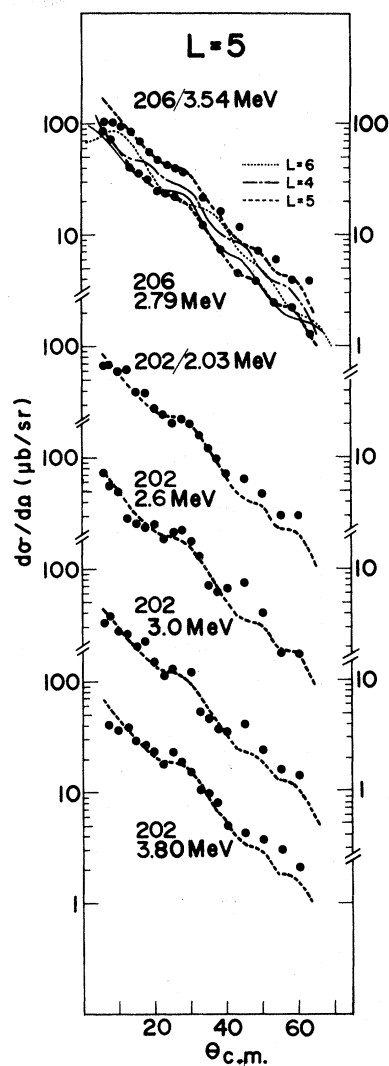


FIG. 6. Experimental differential cross sections for the $L=5$ transitions. See the captions to Figs. 2, 3, and 5.

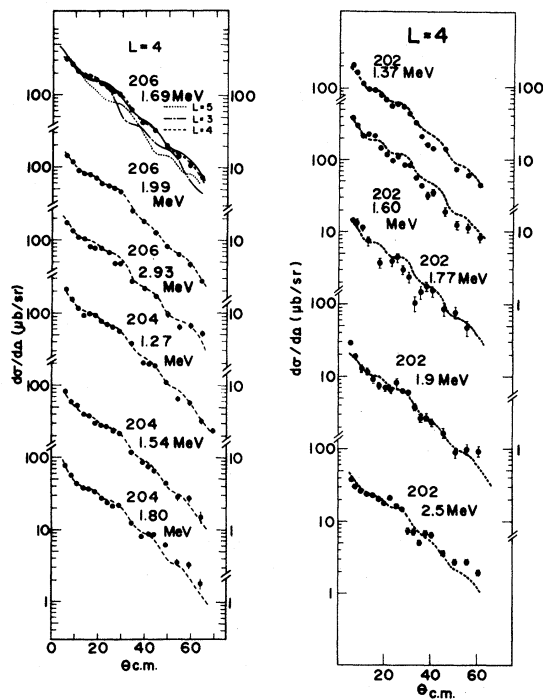


FIG. 5. Experimental differential cross sections for the $L=4$ transitions. See the captions to Figs. 2 and 3. A comparison of experimental angular distribution shapes for alternate values of the transferred L ($=3$ by a dashed and dotted line and $=5$ dotted line) is shown.

of the well-separated peak positions is estimated to be -15 and $+10$ keV from comparison of the present peak energies with those cited in Ref. 11. Overlapping peaks were separated by the same code, and the error of such a peak position is ± 30 keV. The assignments were made in comparison of the experimental differential cross sections with the zero-range DWBA approximation (code DWUCK-4, Ref. 12). Optical parameters are listed in Table I. For the proton channel, optical parameters of Becchetti

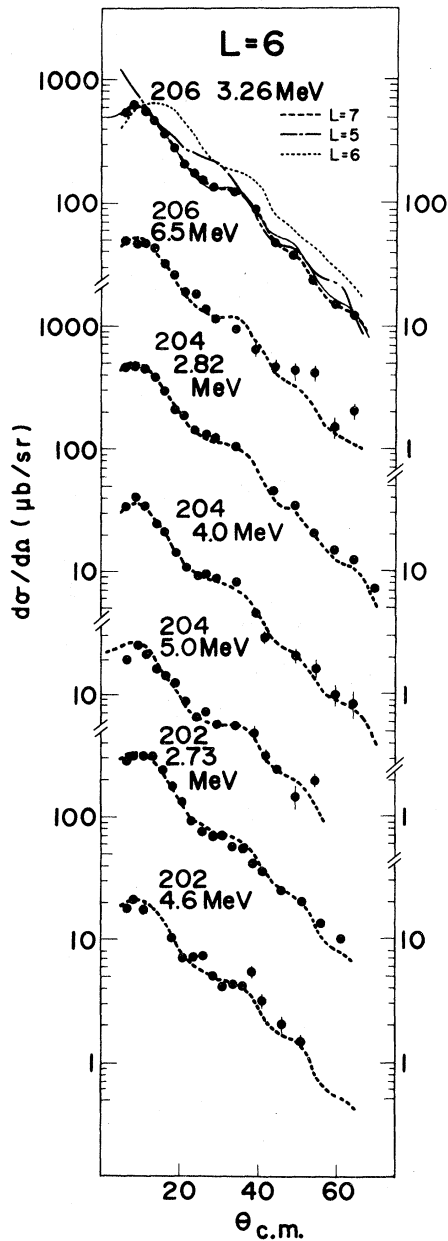


FIG. 7. Experimental differential cross sections for the $L=6$ transitions. See the captions to Figs. 2, 3, and 5.

and Greenlees¹⁰ were used with a somewhat deeper volume-type real potential (V_R) which gave better agreement with the observed angular distributions of proton-elastic scattering on ^{208}Pb . For the triton channel, Flynn's parameters,¹³ which have been successfully employed by many authors for the analyses of the (p,t) data at various proton energies ranging from 20 to 52 MeV,¹⁴ were used. Flynn *et al.*¹³ have reported two sets of parameters differing in the real-well parameters: $r_R=1.24$ fm, $V_R=150$ MeV and $r_R=1.16$ fm, $V_R=167$ MeV. Both angular dis-

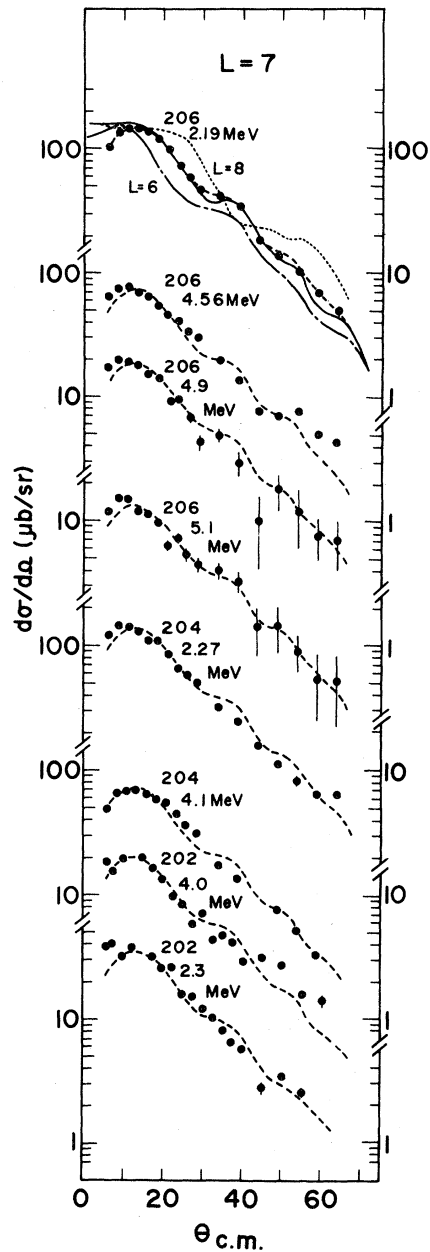


FIG. 8. Experimental differential cross sections for the $L=7$ transitions. See the captions to Figs. 2, 3, and 5.

tributions calculated from these sets show a similar pattern, but the absolute cross sections for an $L=2$ transition are about 60% larger for the latter set than those for the former. For the $L=0$ ground state transition, the cross sections agree well with each other between the two sets of parameters. We use here the latter family. The bound-state wave functions are constructed by varying the neutron well depth so as to give the binding energy of a single neutron which was obtained from the compilation¹⁵ by Schmorak and Auble for ^{207}Pb .

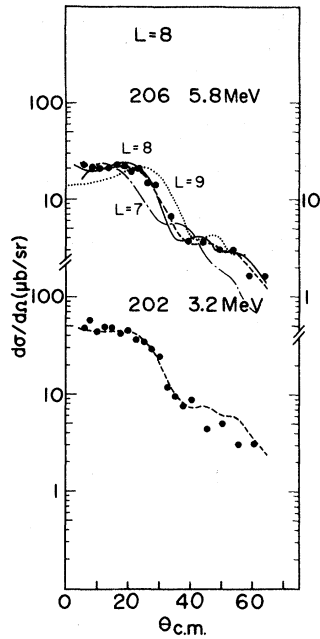


FIG. 9. Experimental differential cross sections for the $L=8$ transitions. See the captions to Figs. 2, 3, and 5.

The excitation energies, spin and parity assignments, and relative transition strengths determined from the present experiment are presented in Tables II–IV. Excitation energies and spin-parity assignments by Lanford *et al.*⁶ are also listed for comparison. “Relative cross section” in the tables means the relative one normalized to the lowest state within each L group of ^{206}Pb excited by the $^{208}\text{Pb}(p,t)^{206}\text{Pb}$ reaction. The experimental energy-level diagrams for the three nuclei are illustrated in Fig. 12. It can be seen that the level ordering is generally the same whereas the level spacing becomes smaller as the neutron number decreases. The relative strengths for the lowest excited states of a given

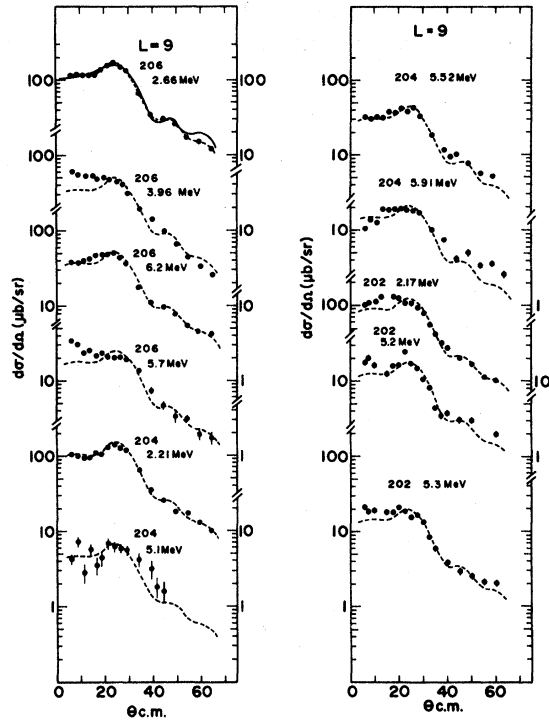


FIG. 10. Experimental differential cross sections for the $L=9$ transitions. See the captions to Figs. 2 and 3.

L value are presented in Fig. 13, which shows that the $L=0$ transition strength remarkably increases but almost all strengths leading to the $J^\pi \neq 0^+$ states lay at constant values as one goes away from the closed shell nucleus, from ^{206}Pb to ^{202}Pb .

IV. SHELL MODEL CALCULATION

The present shell-model calculation for ^{206}Pb is similar to that of True.^{1,2} Parameters of the harmonic-oscillator potential were determined in such a way that the depth of the potential at the nuclear surface becomes the same value as that of a Woods-Saxon potential, which describes the neutron-bound state in ^{206}Pb . The unperturbed single-particle levels were obtained from the experimental results¹⁵ for ^{207}Pb as illustrated in Fig. 14.

TABLE I. Values of optical-model parameters used in analyses of the (p,t) reaction.

	V_R (MeV)	r_R (fm)	a_R (fm)	W_V (MeV)	r_I (fm)	a_I (fm)	W_S (MeV)	V_{so} (MeV)	r_{so} (fm)	a_{so} (fm)	r_C (fm)
Proton	50.1	1.17	0.75	8.60	1.32	0.66	4.9	6.2	1.01	0.75	1.25
Triton	167.0	1.16	0.752	10.3	1.498	0.817					
Neutron	a	1.25	0.75			$\lambda=25$					

^aAdjusted so as to yield the binding energy of a single neutron ($Sn + Ej$), where Sn is the separation energy of a neutron from ^{208}Pb and Ej is the single-particle energy of the j orbit illustrated in Fig. 14.

TABLE II. $^{208}\text{Pb}(p,t)^{206}\text{Pb}$ reaction data: excitation energies, spin and parity assignments, relative cross sections, and comparisons with the results previously reported.

Excitation energy (MeV)	Present results		Lanford (Ref. 6)	
	J^π	Relative cross section	Excitation energy (MeV)	J^π
0.0	0^+	1	0.0	0^+
0.80	2^+	1	0.804	2^+
1.17	0^+	0.13	1.167	0^+
			1.339	3^+
1.46	2^+	0.15	1.466	2^+
1.69	4^+	1	1.684	4^+
			1.783	2^+
1.99	4^+	0.42	1.997	4^+
			2.147	2^+
2.19	7^-	1	2.199	7^-
			2.314	0^+
			2.379	
2.40	2^+	0.10	2.421	2^+
			2.644	3^-
2.66	9^-	1	2.655	9^-
2.79	5^-	1	2.780	5^-
			2.872	
			2.865	
2.93	4^+	0.51	2.928	4^+
			2.979	
			3.014	5^-
			3.119	
			3.193	
3.26	6^+	1	3.256	6^+
			3.390	(7^-)
			3.452	
3.54	5^-	0.50	3.516	
			3.603	2^+
3.77	2^+	0.22	3.765	(7^+)
3.96	$9^-, 8^+$	0.29, 1	3.958	4^+
			4.113	4^+
4.16	3^-	1	4.140	
			4.225	
			4.484	
4.56	7^-	0.49		
4.9	7^-	0.12		
5.1	7^-	0.08		
			5.317	
			5.348	
			5.383	
5.41	11^-	1		
5.7	$9^- + 3^-$ or 4^+	0.14		
5.8	8^+	0.44		
6.2	9^-	0.30		
6.5	6^+	0.09		

For the two-body force, we employ a phenomenological nucleon-nucleon interaction of a Gaussian shape. Here, we deal with only the singlet-even type interaction given by Eq. (1):

$$V(r) = V_0 \exp(-r^2/\beta^2) \quad (1)$$

with $V_0 = -32.5$ MeV and $\beta = 1.85$ fm. These parameters have been determined so as to yield the

TABLE III. $^{206}\text{Pb}(p,t)^{204}\text{Pb}$ reaction data: excitation energies, spin and parity assignments, relative cross sections, and comparison with the results previously reported.

Excitation energy (MeV)	Present results		Lanford (Ref. 6)	
	J^π	Relative cross section	Excitation energy (MeV)	J^π
0.0	0^+	1.59	0.0	0^+
0.90	2^+	0.67	0.899	2^+
1.27	4^+	0.53	1.274	4^+
			1.351	2^+
1.54	4^+	0.20	1.563	4^+
			1.582	
1.7	2^+	0.09	1.663	2^+
			1.728	0^+
1.80	4^+	0.20	1.816	4^+
			1.958	2^+
			2.103	2^+
			2.156	
2.21	9^-	0.81	2.186	9^-
2.27	7^-	0.93	2.257	$J=5+J=7$
			2.399	(7^-)
2.5	2^+	0.24	2.430	
			2.505	5^-
2.6	3^-	1.35	2.620	
			2.660	
2.82	6^+	0.83	2.808	6^+
			2.829	
			2.898	4^+
3.1	2^+	0.11	3.147	
3.2	2^+	0.11	3.226	
3.42	3^-	0.90		
3.81	2^+	0.09		
4.0	6^+	0.06	3.949	
4.1	7^-	0.50		
4.85	11^-	0.57		
5.0	6^+	0.04		
5.1	9^-	0.39		
5.52	9^-	0.12		
5.91	9^-	0.05		

effective range $r_{\text{eff}}=2.65$ fm, which has been obtained from the free nucleon-nucleon scattering.¹⁶ The radial integral in the interaction matrix elements was analytically calculated by expanding the nucleon-nucleon interaction into a polynomial.

In the cases of ^{204}Pb and ^{202}Pb , the matrix elements of the four- or six-body system were obtained from those of the two-body system with the aid of fractional parentage coefficients. Since the interaction between the components with large seniorities is weak in our case, the present model space consists of limited values of seniority; i.e., we take the components whose seniorities are zero for $J^\pi=0^+$ states, and two for $J^\pi \neq 0^+$ states.

We have calculated the wave functions of the

natural parity states of ^{206}Pb and ^{204}Pb , and the 0^+ states in ^{202}Pb . The eigenvalues and eigenfunctions for ^{206}Pb are listed in Table V. It should be noticed in Table V for the later discussions that the $(p_{1/2})^2$ component, which changes rapidly with the decrease in the neutron number of the targets, is a main component for the ground state transition and that the $(p_{1/2}, i_{13/2})$ component is the major part of the transition to the lowest 7^- state. The prominent part of the lowest 6^+ state is $(f_{5/2}, f_{7/2})$. The eigenvalues of ^{204}Pb and the spectroscopic amplitudes of the $^{206}\text{Pb}(p,t)^{204}\text{Pb}$ reaction are shown in Table VI, where a spectroscopic amplitude is divided by $(2L+1)^{1/2}$ for the sake of direct comparison with the eigenfunction in Table V. The present shell-

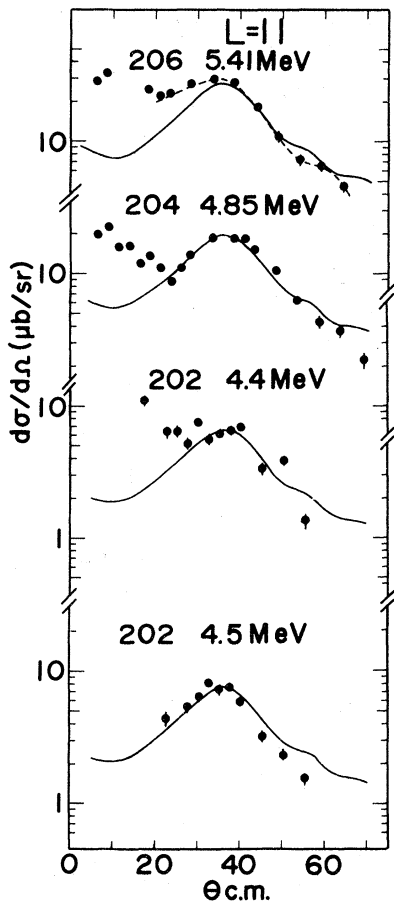


FIG. 11. Experimental differential cross sections for the $L = 11$ transitions. See the captions to Figs. 2 and 3.

model calculation indicates that a substantial rearrangement of two-hole components of $(p_{1/2}, i_{13/2})$, $(f_{5/2}, i_{13/2})$, and $(p_{3/2}, i_{13/2})$ takes place for the lowest 7^- state, as will be discussed later in Sec. V. The calculated results for the $^{208,206}\text{Pb}(p,t)^{206,204}\text{Pb}$ reactions are listed in Tables V and VI. The wave function of the ground state of ^{204}Pb and the spectroscopic amplitude of the $^{204}\text{Pb}(p,t)^{202}\text{Pb}(\text{g.s.})$ reaction are listed in Tables VII and VIII, respectively. Recently, our wave functions were employed successfully by Toba *et al.*¹⁷ to explain analyzing powers $A(\theta)$ for the $^{208}\text{Pb}(\bar{p},t)^{206}\text{Pb}(0_g^+ \text{ and } 0_2^+)$ reactions.

V. COMPARISON OF EXPERIMENTAL RESULTS WITH SHELL-MODEL PREDICTIONS

A. Excitation energies

Figure 15 shows the comparison of the experimental level diagram of ^{206}Pb with the theoretical

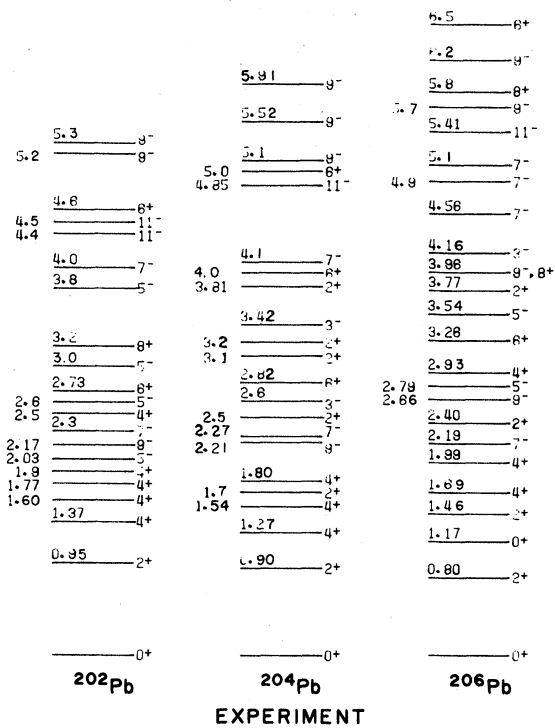


FIG. 12. Excitation energies and J^π values of levels observed in the present investigation.

predictions from the shell-model calculations by Kuo and Herling,³ True,² and the present authors. We choose the states which have transition strengths larger than 0.01 relative to that of the ground-state transitions. The states, which were predicted to have the strong relative strength by Kuo and Her-

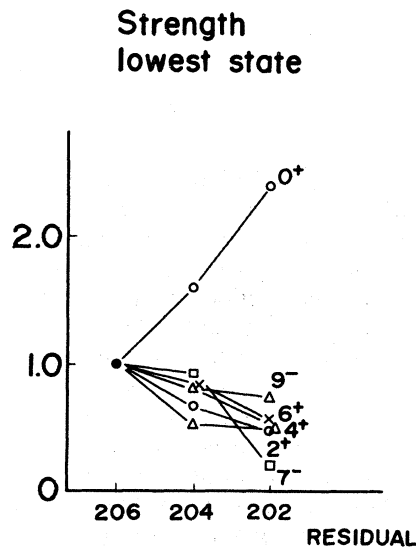


FIG. 13. Isotope dependence of triton strengths leading to the lowest state of $J^\pi = 0^+, 2^+, 4^+, 6^-,$ and 9^- .

TABLE IV. $^{204}\text{Pb}(p,t)^{202}\text{Pb}$ reaction data: excitation energies, spin and parity assignments, relative cross sections, and comparison with the results previously reported.

Excitation energy (MeV)	Present results		Lanford (Ref. 6)	
	J^π	Relative cross section	Excitation energy (MeV)	J^π
0.0	0^+	2.39	0.0	0^+
0.95	2^+	0.47	0.961	2^+
1.37	4^+	0.49	1.383	4^+
			1.584	(2^+)
1.60	4^+	0.10	1.623	4^+
			1.657	2^+
1.77	4^+ or 2^+	0.04	1.798	
			1.815	
1.9	4^+	0.06	1.915	4^+
2.03	5^-	0.50	2.040	5^-
2.17	9^-	0.73	2.172	9^-
			(2.185)	
			2.202	
2.3	7^-	0.22	(2.307)	
			2.364	
			2.389	
2.5	4^+	0.12	2.516	4^+
2.6	5^-	0.42		
			2.666	4^+
2.73	6^+	0.57	2.747	6^+
3.0	5^-	0.26	2.995	
			3.131	
			3.180	4^+
3.2	8^+	0.93		
3.8	5^-	0.39		
4.0	7^-	0.14		
4.4	11^-	0.23		
4.5	11^-	0.26		
4.6	6^+	0.04		
5.2	9^-	0.10		
5.3	9^-	0.12		

ling, are also illustrated for comparison, though in general it seems that they are depressed by 300 keV in excitation energy in comparison with the other two calculations.

True has calculated the states of $E_x \leq 3.4$ MeV, employing a phenomenological Gaussian-shaped potential for a singlet-even force, which takes into account the quadrupole interaction as a perturbation. We employed a pure singlet-even interaction without adjustment, and obtained results similar to True's predictions except for the position of the lowest 2^+ state in ^{206}Pb . Good agreement between the shell model and the experiments for the level diagram of ^{206}Pb has been obtained. Excitation energies of the observed levels are reproduced within an uncertainty of 220 keV up to the 11^- state at $E_x = 5.4$ MeV.

Figure 16 shows a similar comparison, where good agreement is seen for the level diagram of

natural parity states in ^{204}Pb within an uncertainty of 250 keV, except for the lowest 3^- state.

B. Transition strengths

The cross section calculated in the code DWUCK is connected with the experimental cross section by

$$\left[\frac{d\sigma}{d\Omega} \right]_{\text{exp}} = \frac{D_0^2 (\frac{1}{2}\pi\Delta^2)^{3/2}}{2L+1} \epsilon \left[\frac{d\sigma}{d\Omega} \right]_{\text{DWUCK}}, \quad (2)$$

where D_0^2 is the zero-range normalization factor and Δ is the rms radius of the triton. From systematic studies of the (t,p) and (p,t) reactions, these factors were determined to be $\Delta = 1.7$ fm and $D_0^2 = 22 \text{ MeV}^2 \text{ fm}^3$ (Ref. 18). The parameter ϵ is an enhancement factor and gives information about the degree of "enhancement" beyond the framework of the shell model. The factor $(d\sigma/d\Omega)_{\text{DWUCK}}$ in Eq.

TABLE V. Eigenvalues and eigenfunctions of natural-parity states in ^{206}Pb .

Eigen-value (MeV)	Excitation energy (MeV)	$P_{1/2}^2$	$f_{3/2}^2$	$P_{3/2}^2$	$i_{13/2}^2$	$f_{7/2}^2$	$h_{9/2}^2$	$P_{3/2}f_{7/2}$	$i_{13/2}^2$	$f_{7/2}^2$
$J^\pi=0^+$										
-0.957	0.0	0.795	0.390	0.393	0.165	0.167	0.076			
0.247	1.204	-0.534	0.786	0.122	0.204	0.183	0.082			
$J^\pi=2^+$										
-0.201	0.756	$P_{1/2}f_{5/2}$	$P_{1/2}P_{3/2}$	$f_{5/2}^2$	$f_{5/2}P_{3/2}$	$f_{5/2}f_{7/2}$	$P_{3/2}^2$	$P_{3/2}f_{7/2}$	$i_{13/2}^2$	$f_{7/2}^2$
0.429	1.385	-0.703	0.546	-0.255	0.174	0.063	-0.213	-0.207	-0.079	-0.083
0.906	1.862	-0.621	-0.760	-0.002	0.046	0.0	0.183	-0.041	0.0	0.0
1.383	2.340	-0.249	0.194	0.937	-0.081	-0.063	0.002	0.047	0.059	0.069
2.560	3.517	-0.169	0.096	-0.157	-0.959	-0.014	0.085	0.098	0.026	0.014
2.854	3.810	-0.040	0.268	-0.063	0.133	-0.014	0.950	0.035	0.022	0.012
2.896	3.853	-0.057	0.019	-0.032	0.050	-0.565	-0.025	0.537	0.663	0.119
		0.071	-0.021	-0.010	-0.061	-0.735	0.026	0.450	-0.681	0.036
$J^\pi=3^-$										
3.421	4.377	$i_{13/2}f_{7/2}$	$i_{13/2}h_{9/2}$							
5.070	6.027	-0.997	0.075	0.997						
$J^\pi=4^+$										
0.768	1.725	$P_{1/2}f_{7/2}$	$f_{5/2}^2$	$f_{5/2}P_{3/2}$	$f_{5/2}f_{7/2}$	$P_{3/2}f_{7/2}$	$i_{13/2}^2$	$f_{7/2}^2$		
1.137	2.093	0.284	-0.571	0.732	0.134	-0.153	-0.067	-0.069		
2.111	3.067	0.134	0.811	0.565	-0.002	-0.065	-0.009	0.001		
4.553	5.510	-0.898	-0.087	0.359	-0.143	0.155	0.074	0.042		
		0.031	-0.029	0.025	0.080	-0.044	-0.032	0.988		
$J^\pi=5^-$										
2.058	3.014	$f_{5/2}i_{13/2}$	$P_{3/2}i_{13/2}$	$i_{12/2}f_{7/2}$	$i_{13/2}h_{9/2}$					
2.275	3.232	-0.766	0.632	0.120	0.022					
		0.641	0.765	0.060	0.007					
$J^\pi=6^+$										
2.211	3.168	$f_{5/2}f_{7/2}$	$i_{13/2}^2$	$f_{7/2}^2$						
3.100	4.057	0.978	-0.135	-0.113						
4.607	5.564	-0.149	-0.982	-0.007						
		0.104	-0.017	0.991						
$J^\pi=7^-$										
1.393	2.349	$P_{1/2}i_{13/2}$	$f_{5/2}i_{13/2}$	$P_{3/2}i_{13/2}$	$i_{13/2}f_{7/2}$	$i_{13/2}h_{9/2}$				
2.087	3.044	-0.964	-0.198	0.159	0.069	0.022				
2.443	3.400	-0.232	0.951	-0.193	-0.063	-0.024				
3.848	4.804	0.116	0.227	0.966	0.040	0.009				
		-0.048	-0.066	-0.063	-0.993	-0.061				

TABLE V. (Continued.)

Eigen-value (MeV)	Excitation energy (MeV)		
$J^\pi = 8^+$		$h_{9/2}^2$	
3.140	4.096	$f_{7/2}h_{9/2}$	-0.023
5.383	6.340		0.050
$J^\pi = 9^-$		$i_{13/2}^2$	
1.787	2.744	$f_{5/2}i_{13/2}$	-0.998
3.884	4.841		-0.056
4.870	5.827	$i_{13/2}f_{7/2}$	-0.062
			-0.076
			-0.995
$J^\pi = 11^-$		$i_{13/2}h_{9/2}$	
3.176	4.132		1.0

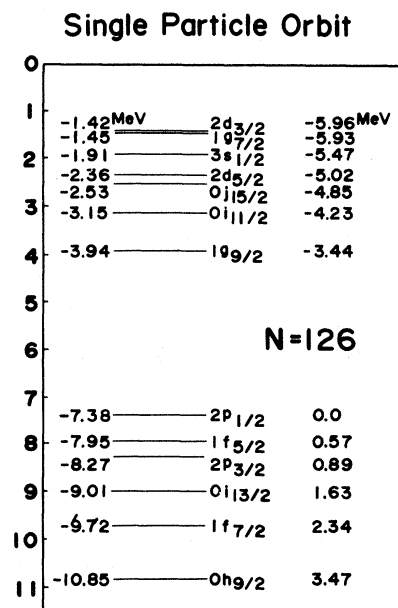


FIG. 14. Single particle states and energies used in the DWBA calculation and for the shell-model calculation.

(2) contains the spectroscopic amplitudes as well. Following Shepard *et al.*,¹⁹ the numerical relationship of $(d\sigma/d\Omega)_{\text{exp}}$ to $(d\sigma/d\Omega)_{\text{DWUCK}}$ is for pickup of neutrons in a single shell:

$$\left(\frac{d\sigma}{d\Omega} \right)_{\text{exp}} \left(\frac{\text{mb}}{\text{sr}} \right) = \frac{2127}{2L+1} \epsilon S_{AB} \left(\frac{d\sigma}{d\Omega} \right)_{\text{DWUCK}} \left(\frac{\text{fm}^2}{\text{sr}} \right), \quad (3)$$

where S_{AB} is the spectroscopic factor for the transition between pure configurations, and here in Eq. (3) $(d\sigma/d\Omega)_{\text{DWUCK}}$ does not contain $S_{AB}^{1/2}$.

In order to examine the validity of the present model space, the experimental cross sections summed over the transitions with a given L transfer are compared with the summed ones predicted from the DWBA for pure configurations currently allowed, and are shown in Fig. 17. The fact that almost all of the ϵ factors are close to unity justifies the present model space, since a summed cross section should be independent of the configuration mixing from the simple sumrule for the (p,t) reaction.

Meanwhile, the differential cross section for a two-nucleon transfer reaction like the (p,t) reaction is described by the sum of the product of the reaction amplitudes and the spectroscopic amplitudes over the two-hole configurations which are allowed for a given L transfer within the model space.²⁰ A reaction amplitude, in general, is a complex number.

TABLE VII. Wave function of the ground state of ^{204}Pb .

	$f_{5/2}^2$	$p_{3/2}^2$	$i_{13/2}^2$	$f_{7/2}^2$	$h_{9/2}^2$
$p_{1/2}^2$	0.598	0.538	0.201	0.207	0.089
$f_{5/2}^2$	0.196	0.341	0.133	0.136	0.060
$p_{3/2}^2$		0.161	0.123	0.129	0.056
$i_{13/2}^2$			0.035	0.053	0.024
$f_{7/2}^2$				0.033	0.024
$h_{9/2}^2$					0.007

In the case of the present study, however, it was empirically found that the relative phase between a pair of the spectroscopic amplitudes is quite close to 0 or 180 deg, i.e., the relative phase is nearly 0° when the two components are constructive for the resultant cross section (the signs of the reaction amplitude are identical), and 180° when they are destructive (the signs are opposite). (See the Appendix.)

The theoretical cross section at an angle in the

center of mass system is obtained as follows: We calculate reaction amplitudes by using the code DWUCK-4 for all pure configurations, then we sum up products of the square root of the reaction amplitude and the spectroscopic amplitude for all relevant two-hole configurations listed in Tables V and VI and Table VIII, taking into account the sign of the reaction amplitude, and finally we find the cross section by squaring the summed value.

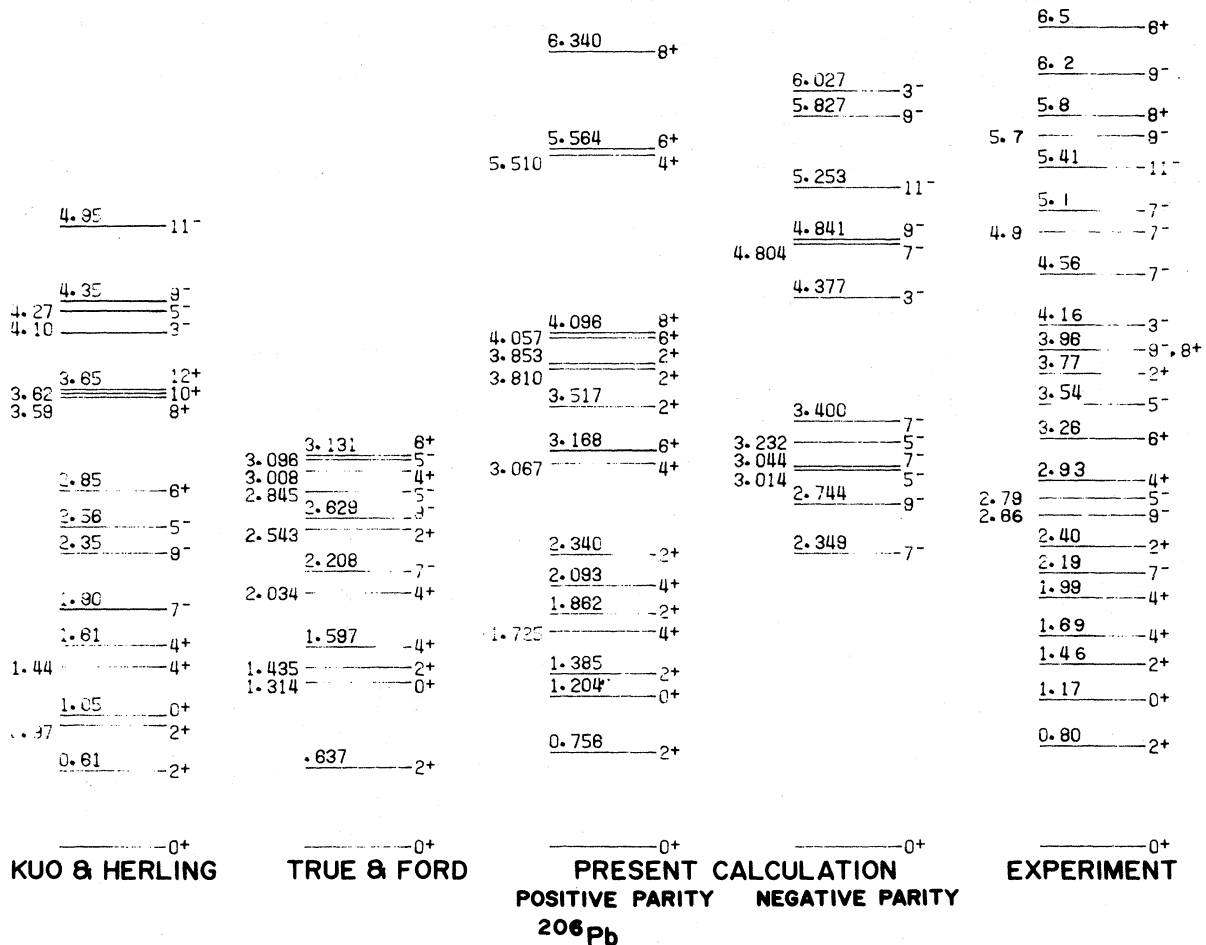


FIG. 15. Comparison of excitation energies obtained from the calculations of Refs. 1 and 3, the present calculation, and the experimental results for ^{206}Pb .

TABLE VIII. Spectroscopic amplitude of the $^{204}\text{Pb}(p,t)^{202}\text{Pb}(\text{g.s.})$ reaction.

$p_{1/2}^2$	$f_{5/2}^2$	$p_{3/2}^2$	$i_{13/2}^2$	$f_{7/2}^2$	$h_{9/2}^2$
-0.460	-0.902	-0.811	-0.353	-0.370	-0.156

Thus, an enhancement factor can be deduced, even in a case where the configuration mixing takes place in the initial and/or final states, from a comparison of the experimental cross section with the theoretical value through the treatment mentioned before. The method of comparing the experimental results with the theoretical predictions for the individual states is as follows: First we check the absolute cross sections of the $^{208}\text{Pb}(p,t)^{206}\text{Pb}$ reaction which lead to the lowest states in ^{206}Pb for each J^π , then we examine the distribution of the relative strengths of tritons which excite the other states in ^{206}Pb and all the states in ^{204}Pb and ^{202}Pb for each L transition. Figure 18 shows the L dependence of the ϵ factor for transitions to the lowest state for each L transition as mentioned above. The values of the ϵ factor are very close to unity except for the cases of the lowest 3^- and 8^+ states. In Figs. 19–21, we present the distribution of the strengths for individual states excited by transitions of a given L value from 0 to 11 in the $^{208,206,204}\text{Pb}(p,t)^{206,204,202}\text{Pb}$ reactions.

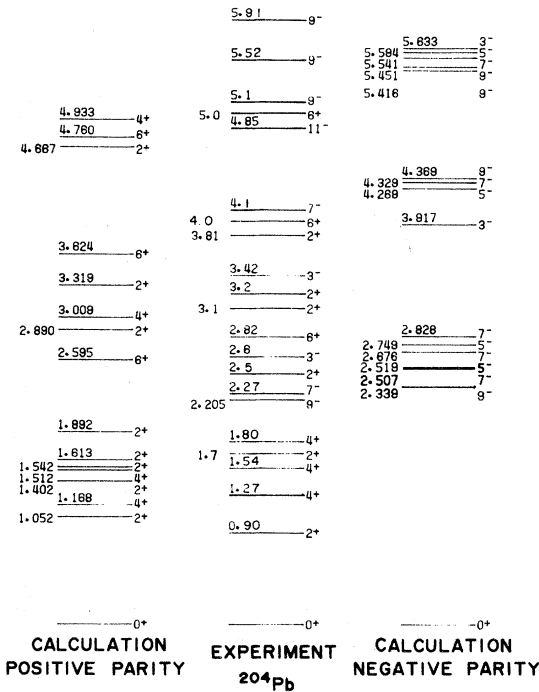


FIG. 16. Comparison of the calculated excitation energies with the experimental results for ^{204}Pb .

enhancement factor
 $^{208}\text{Pb}(p,t)^{206}\text{Pb}$
sum

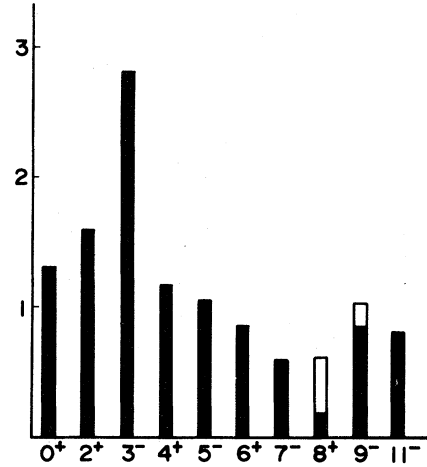


FIG. 17. Distribution of enhancement factors obtained from summed cross sections. Blank parts in 8^+ and 9^- are due to the choice of J^π for the 3.96-MeV state.

VI. DISCUSSION

As mentioned before, the positions of excited states populated by the (p,t) reactions on $^{208,206,204}\text{Pb}$ at $E_p=52$ MeV are well reproduced by the present

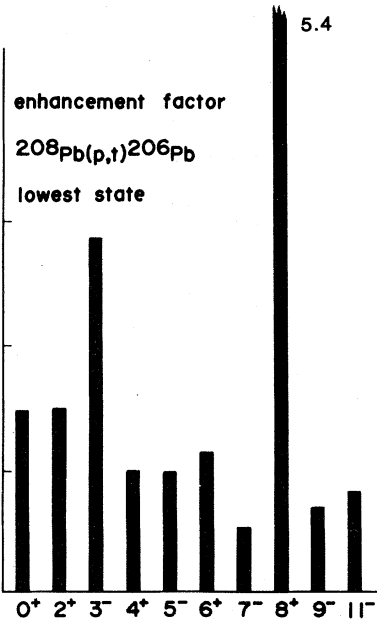


FIG. 18. Distribution of enhancement factors of the transition to the lowest states for each J^π value in ^{206}Pb : 0^+ state at 0.0 (in MeV); 2^+ state at 0.80; 4^+ state at 1.69; 5^- state at 3.54; 6^+ state at 3.26; 7^- state at 2.19; (8^+) state at 3.96; 9^- state at 2.66; 11^- state at 5.41.

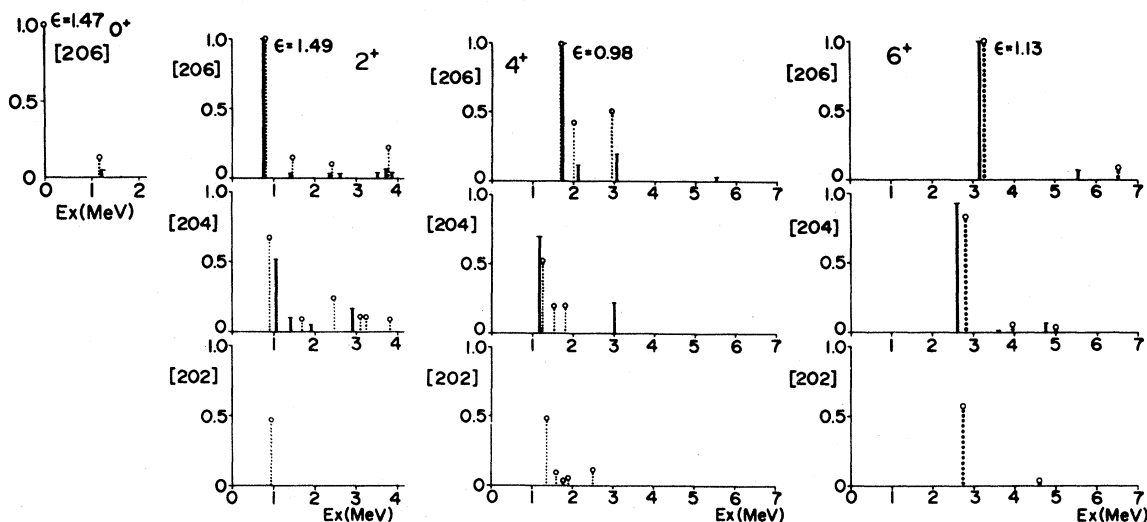


FIG. 19. Comparison of the relative enhancement factor and excitation energies between the shell model predictions and the experimental results for 0^+ , 2^+ , 4^+ , and 6^+ states in ^{206}Pb , ^{204}Pb , and ^{202}Pb . Enhancement factors are normalized to those for the transitions to g.s., 0.80-MeV 2^+ , 1.69-MeV 4^+ , and 3.26-MeV 6^+ states in ^{206}Pb . The solid and dotted lines indicate the theoretical and experimental strengths, respectively. No excited 0^+ state was observed in ^{204}Pb and ^{202}Pb .

shell-model calculation. In addition to the transition strength to the lowest state within a given transfer- L value in the $^{208}\text{Pb}(p,t)^{206}\text{Pb}$ reaction, good agreement has been obtained between the theory and the experimental results for the transitions to other states in ^{206}Pb and all states in ^{204}Pb and ^{202}Pb .

A. 0^+ , 2^+ , 4^+ , and 6^+ states

The isotope dependence of transition strengths populating the lowest 0^+ , 2^+ , 4^+ , and 6^+ states in the residual nuclei of ^{206}Pb , ^{204}Pb , and ^{202}Pb is shown in Fig. 22 in comparison with the theoretical

relative cross sections predicted from the shell model. From this figure one can find remarkable agreements between the shell-model calculation and the experiment. Although a simple pairing-vibration model predicts the relative strengths of 1:2:3 for the ground state transitions, the experimental ratios of the cross sections $I(^{208}\text{Pb}; \text{target}): I(^{206}\text{Pb}): I(^{204}\text{Pb})$ are 1:1.59:2.39 for the ground state transitions, and are well explained by the present shell-model calculation. Ui *et al.*²¹ have carried out a calculation based on a model which consisted of degenerate many- j single-particle levels and degenerate hole levels with an energy gap, taking into ac-

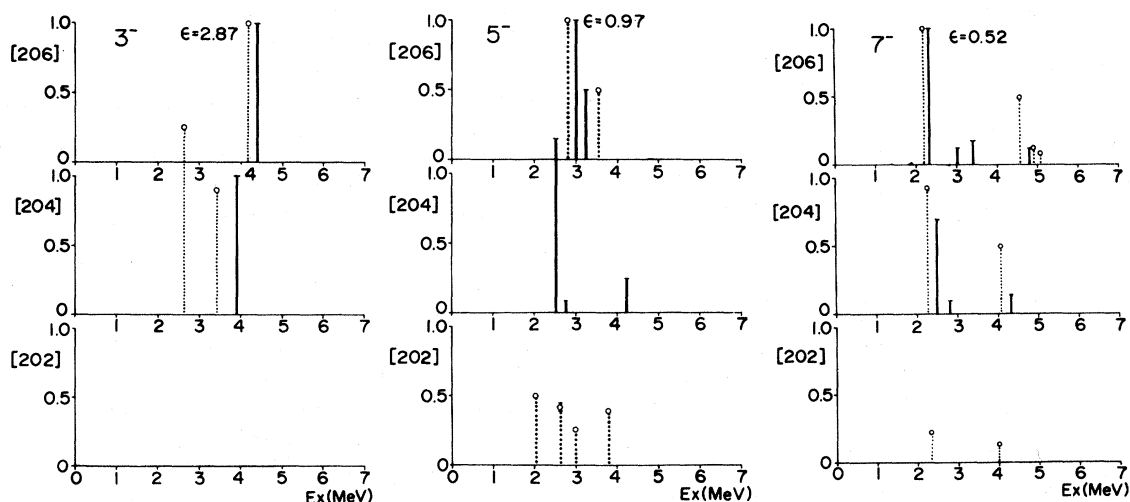


FIG. 20. Comparisons for 3^- , 5^- , and 7^- states. See the caption to Fig. 19.

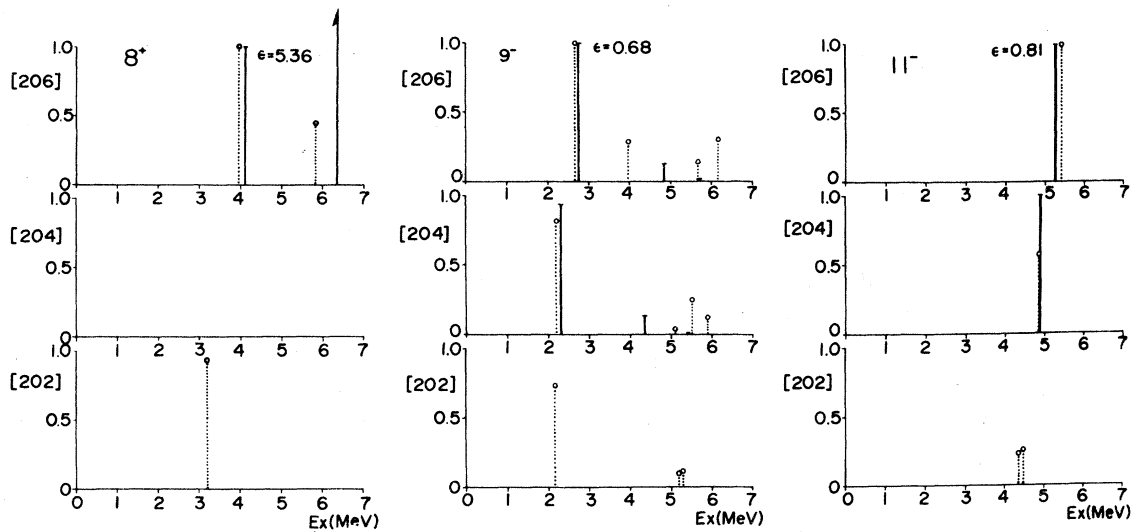


FIG. 21. Comparisons for 9^- , 8^+ , and 11^- states. See the caption to Fig. 19.

count the pairing interactions, and obtained good agreement with experimental results. Recently, Broglia *et al.*²² reported a microscopic study of the role

of pairing vibrations in the (t,p) and (p,t) data around ^{208}Pb . They obtained that the ratios of the cross sections were 2.7:4.5:6.2 (1:1.67:2.30) from the Tamm-Dancoff approximation (TDA) and 4.8:8.5:11.1 (1:1.64:2.31) from the Bardeen-Cooper-Schrieffer (BCS) theory.

Meanwhile, it is predicted from the simple pairing-vibration model for the transitions to the 2^+ and 4^+ states that these cross sections are constant with respect to the change of the target mass. Experimental results, however, show that the cross sections leading to the 2^+ and 4^+ states decrease with the decrease of the target mass. Such behavior is interpreted by the lack of occupation of the $p_{1/2}$ shell in ^{206}Pb and ^{204}Pb , while this component is a dominant part in the $^{208}\text{Pb}(p,t)^{206}\text{Pb}$ reaction. Indeed the configurations $(p_{1/2}f_{5/2})_{2^+}$ and $(p_{1/2}f_{7/2})_{4^+}$ give large cross sections. Furthermore, the experimental distribution of the relative strengths leading to the 6^+ states is nearly constant and this fact is well described by the shell-model treatment, where the effect of the $(f_{5/2}f_{7/2})$ component is significant.

In Fig. 19 the position and the strength for the excited 0^+ state only for ^{206}Pb is illustrated together with the theoretical prediction, since no excited 0^+ states were observed in ^{204}Pb and ^{202}Pb .

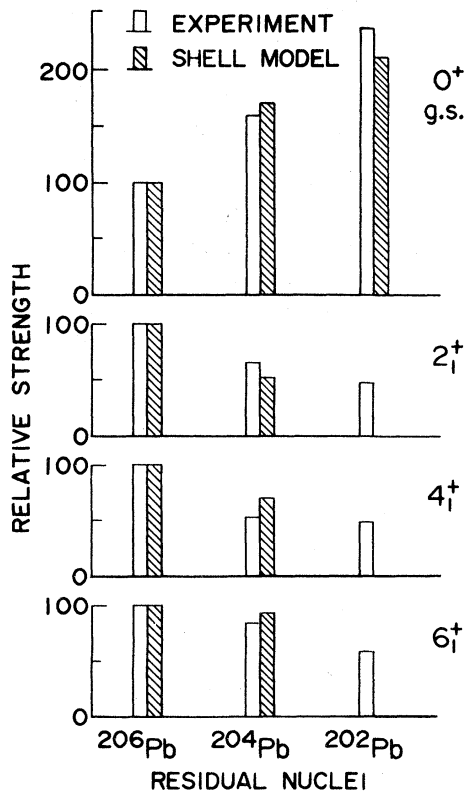


FIG. 22. Comparisons of the experimental cross sections with the relative cross sections predicted from the shell model (for the ground-state transitions and for those to the lowest 2^+ , 4^+ , and 6^+ states in ^{206}Pb and ^{204}Pb).

B. 3^- states

The relative strengths of $L=3$ transitions are illustrated in Fig. 20. The enhancement factor of the transition to the lowest 3^- state and that of the summed cross section are too large to be explained by the two-hole configurations, and this fact suggests a contribution from other collective degrees of freedom.

C. 5^- states

The relative strengths of the $L=5$ transitions are also displayed in Fig. 20. Two $J^\pi=5^-$ states were observed at 2.79 and 3.54 MeV in ^{206}Pb , and the shell-model calculation predicts two 5^- states in 3.01 and 3.23 MeV. The predicted 3.01-MeV state may correspond to the observed 2.79-MeV state. We could not, however, assign the observed 3.54-MeV state to be a candidate of the calculated 3.232-MeV state, since the theoretical value for negative-parity states in this excitation energy region is, systematically, 100 keV higher than the experimental one as seen in Fig. 15. Lanford *et al.*⁶ have reported five 5^- states including a 3.01-MeV state, which gives a better agreement with our calculation. No 5^- states were observed for ^{204}Pb in the present measurements. The 2.25 MeV level reported in Ref. 6 might be masked in the present measurement by the higher spin and strong $L=9$ and $L=7$ transitions to the 2.21- and 2.27-MeV states, respectively.

D. 7^- and 9^- states

Figure 20 illustrates the relative strengths for the $L=7$ transitions, and strengths for the $L=9$ transitions are shown in Fig. 21. Contrary to other J^π levels, the excitation energy of the lowest 7^- state increases with the decrease in the neutron number, in agreement with the present shell-model calculation. This is understood by the fact that the main component of the 7^- state is $(p_{1/2}, i_{13/2})$ in ^{206}Pb , while a substantial rearrangement of two-hole components in the wave function occurs in ^{204}Pb . (See Tables V and VI.)

By examining Figs. 20 and 21, one can notice that a number of strongly excited 7^- and 9^- levels are populated in the higher excitation-energy region, and that the values of the relative strengths are much larger than predicted ones. The present calculation predicts pure configurations for these highly-excited and high-spin states (see Table V). These experimental results might suggest a drastic configuration mixing caused by another kind of nucleon-nucleon interaction.

E. 8^+ states

The relative strength for $L=8$ transitions is shown in Fig. 21. A tentative assignment is given to the 3.96-MeV state in ^{206}Pb . The pattern of the angular distribution and the excitation energy are well explained by the $L=8$ transition, but the magnitude of the cross section is too large: The enhancement factor is 5.4. To explain this discrepancy, a configuration mixing of $0.9(i_{13/2})^2 + 0.44(f_{7/2}, h_{9/2})$ is needed instead of the pure $(i_{13/2})^2$ configuration, which

was obtained in the present calculation. A comparison of calculated angular distribution shapes for alternate values of the transferred L is shown in Fig. 21.

F. 11^- states

The relative strengths for $L=11$ transitions are illustrated in Fig. 21. Two previously unknown 11^- states were found in ^{202}Pb . Figure 21 shows a systematic behavior of the relative strength and the excitation energy with the decrease in the neutron number. The splitting into two states in ^{202}Pb might be interpreted by the mixing of a high seniority component, since the separation of the two levels is small (80 keV) and the summed cross section has the same magnitude as that for ^{204}Pb .

VII. CONCLUSION

By means of higher-energy incident protons and a highly enriched ^{204}Pb target, a number of previously unreported high-spin states in even lead nuclei were systematically found.

Experimental angular distributions for emitted tritons have been well reproduced by the zero-range DWBA predictions except for the cases of the transition to low-spin states of 0^+ , 2^+ , and 3^- . Consistent explanations have been given for the excitation energies, the level sequences of the even lead isotopes and the enhancement factors for the (p,t) reactions on ^{208}Pb , ^{206}Pb , and ^{204}Pb by the shell-model calculation, where we assumed a singlet-even force for the two-body interaction and the restricted seniorities (zero for 0^+ states and two for $J^\pi \neq 0^+$ ones). A more reliable interaction is needed to explain completely the behavior of the high-lying 7^- , 8^+ , and 9^- states, and the seniority space must be expanded in order to explain the splitting of the 11^- state in ^{202}Pb .

ACKNOWLEDGMENTS

Thanks are due to Professor P. D. Kunz for allowing us to use the code DWUCK-4. The authors appreciate the help of Mr. I. Sugai for the preparation of targets.

APPENDIX

In the case of a transfer process to a state consisting of two configurations, the transition strength is described by

$$|A + Be^{i\phi}|^2, \quad (\text{A1})$$

where A and B are absolute values of the reaction amplitude, and ϕ is the relative phase between the

TABLE IX. Relative phase between the two transfer components.

$L=2$		$\theta=10$ deg			
		$\sigma_{0,1}$	σ_{0+1}	ϕ (deg)	η
0	$p_{3/2}^2$	1.143			
1	$i_{13/2}^2$	0.021	0.919	142	1.08
	$f_{7/2}^2$	0.506	3.123	14	0.99
	$p_{3/2}f_{7/2}$	2.552	0.306	173	1.10
	$f_{5/2}^2$	0.440	2.941	17	0.98
	$p_{1/2}p_{3/2}$	2.430	0.242	178	1.01
	$p_{1/2}f_{5/2}$	1.723	0.093	171	1.58
	$f_{5/2}p_{3/2}$	0.462	3.043	8	1.00
	$f_{5/2}f_{7/2}$	0.133	0.521	166	1.05
$L=4$		$\theta=20$ deg			
0	$f_{7/2}^2$	0.685			
1	$p_{1/2}f_{7/2}$	3.553	7.325	8	1.00
	$f_{5/2}p_{3/2}$	4.483	8.634	9	1.00
	$f_{5/2}f_{7/2}$	0.816	0.09	176	1.55
	$p_{3/2}f_{7/2}$	2.348	0.515	173	1.04
	$f_{5/2}^2$	0.477	2.297	8	1.00
	$i_{13/2}^2$	0.036	0.429	158	1.06
$L=5$		$\theta=25$ deg			
0	$p_{3/2}i_{13/2}$	2.276			
1	$f_{5/2}i_{13/2}$	0.161	3.642	5	1.00
	$i_{13/2}f_{7/2}$	0.713	0.525	165	1.19
$L=6$		$\theta=10$ deg			
0	$f_{7/2}^2$	3.424			
1	$i_{13/2}^2$	0.218	1.949	168	1.02
	$f_{5/2}f_{7/2}$	22.655	8.480	178	1.00
$L=7$		$\theta=10$ deg			
0	$p_{3/2}i_{13/2}$	5.888			
1	$p_{1/2}i_{13/2}$	10.755	0.734	178	1.01
	$f_{5/2}i_{13/2}$	2.486	16.017	3	1.00
	$i_{13/2}f_{7/2}$	2.770	0.637	173	1.10

two configurations. It follows then that

$$\cos\phi = \frac{|A+B^i\phi|^2 - (A^2+B^2)}{2AB} \quad (\text{A2})$$

so that

$$\cos\phi = \frac{\sigma_{0+1} - (\sigma_0 + \sigma_1)}{2\sqrt{\sigma_0\sigma_1}}, \quad (\text{A3})$$

where σ_0 and σ_1 are the transition strengths for each pure configuration, and σ_{0+1} is that for the mixed one when both spectroscopic amplitudes are equal to unity.

We have empirically found that the phase in a complex plane between two components of the transition is very close to 0 or 180 deg in the reactions presently investigated. The values of ϕ obtained from the differential cross section at $\theta_{c.m.} = 10^\circ$ for $L=2, 6, 7$, $\theta_{c.m.} = 20^\circ$ for $L=4$, and $\theta_{c.m.} = 25^\circ$ for $L=5$ transitions are listed in Table IX. An error function (η) in a transition strength, which comes from putting $\phi=0^\circ$ for the transition of $\phi \simeq 0^\circ$ and putting $\phi=180^\circ$ in the case of $\phi \simeq 180^\circ$, is defined by

$$\eta = \frac{\sigma_{0+1}}{(\sqrt{\sigma_0} + \sqrt{\sigma_1 \cos\phi})^2}, \quad (\text{A4})$$

where $\phi=0^\circ$ or 180° . It can be seen from Table IX that most of the values of ϕ lie within 10 deg of 0 to 180 deg, and the values of η are less than 10%. In particular, η is within $\pm 2\%$ when the two configura-

tions are constructive. Consequently, we can take the real reaction amplitude for the evaluation of cross sections by putting the relative phase to be 0 or 180 deg.

*Present address: Nihon Medi-Physics Inc., Takarazuka 665, Japan.

†Present address: Research Center of Ion Beam Technology, Hosei University, Koganei, Tokyo 184, Japan.

¹W. W. True and K. W. Ford, Phys. Rev. 109, 1675 (1958).

²W. W. True, Phys. Rev. 168, 1388 (1968).

³T. T. S. Kuo, and G. H. Herling, Naval Research Laboratory Memorial Report 2258, 1971 (unpublished).

⁴W. A. Lanford and J. B. McGrory, Michigan State University Cyclotron Laboratory Report No. MSUCL-81, 1973 (unpublished); Phys. Lett. 45B, 283 (1973).

⁵S. M. Smith, P. G. Roos, A. M. Bernstein, and C. Moazed, Nucl. Phys. A158, 497 (1970).

⁶W. A. Lanford, Phys. Rev. C 16, 988 (1977).

⁷B. F. Bayman and C. F. Clement, Phys. Rev. Lett. 29, 1020 (1972).

⁸H. Orihara, Y. Ishizaki, G. F. Trentelman, M. Kanazawa, K. Abe, and M. Yamaguchi, Phys. Rev. C 9, 266 (1974).

⁹K. Yagi, H. Ogawa, Y. Ishizaki, T. Ishimatsu, J. Kokame, and K. Matsuda, Nucl. Instrum. Methods 52, 29 (1967).

¹⁰F. D. Becchetti, Jr. and G. W. Greenlees, Phys. Rev.

182, 1190 (1969).

¹¹K. K. Seth, Nucl. Data Sheets B7, 161 (1972).

¹²P. D. Kunz, private communication.

¹³E. R. Flynn, D. D. Armstrong, J. G. Beery, and A. G. Blair, Phys. Rev. 182, 1113 (1969).

¹⁴See, for example, T. Suehiro, J. Kokame, Y. Ishizaki, H. Ogata, Y. Sugiyama, Y. Saji, and I. Nonaka, Nucl. Phys. A220, 461 (1974).

¹⁵M. R. Schmorak and R. L. Auble, Nucl. Data Sheets B5, 207 (1971).

¹⁶H. A. Bethe and P. Morrison, *Elementary Nuclear Theory*, 2nd ed. (Wiley, New York, 1956).

¹⁷Y. Toba, Y. Aoki, H. Iida, S. Kunori, K. Nagano, and K. Yagi, Phys. Lett. 100B, 232 (1981).

¹⁸J. B. Ball, R. A. Auble, and P. G. Roos, Phys. Rev. C 4, 196 (1971).

¹⁹J. R. Shepard, R. Graetzer, and J. J. Kraushaar, Nucl. Phys. A197, 17 (1972).

²⁰I. S. Towner and J. C. Hardy, Adv. Phys. 18, 401 (1969).

²¹H. Ui and H. Sagawa, Prog. Theor. Phys. 49, 491 (1973).

²²B. A. Broglia, R. J. Liotta, B. S. Nilsson, and E. R. Flynn, Nucl. Phys. A343, 24 (1980).